Energy Storage Materials 49 (2022) 509–517

Contents lists available at ScienceDirect

Energy Storage Materials

journal homepage: www.elsevier.com/locate/ensm

A design concept for halogen-free Mg^{2+}/Li^{+}-dual salt-containing gel-polymer-electrolytes for rechargeable magnesium batteries

Peiwen Wang [a], Janina Trück [a,c], Joachim Häcker [d], Anja Schlosser [e], Kathrin Küster [f], Ulrich Starke [f], Leonie Reinders [b], Michael R. Buchmeiser [a,b,*]

[a] Institute of Polymer Chemistry, University of Stuttgart, 70569, Stuttgart, Germany
[b] German Institutes of Textile and Fiber Research (DITF), 73770 Denkendorf, Germany
[c] Daimler AG, 70327 Stuttgart, Germany
[d] Institute of Engineering Thermodynamics, German Aerospace Center, 70569 Stuttgart, Germany
[e] Customcells Holding GmbH, 25524 Itzehoe, Germany
[f] Max Planck Institute for Solid State Research, 70569 Stuttgart, Germany

ARTICLE INFO

Key words:
gel-polymer electrolyte
in-situ crosslinking
halogen-free
room-temperature magnesium-sulfur/ion batteries

ABSTRACT

Polymer-based electrolytes can greatly promote the development of rechargeable metal-sulfur batteries owing to the improved safety and high flexibility; however, liquid electrolytes, which are mostly investigated so far, often hinder practical application due to the severe shuttling effect and possible leakage of the electrolytes. Herein, a new cell design is presented, that bridges the gap between lab cells and application by a novel halogen-free gel-polymer-electrolyte (GPE) with outstanding electrochemical performance. The GPE was prepared *via* an *in-situ* crosslinking reaction between lithium/magnesium borohydrides and poly(tetrahydrofuran). This GPE displays outstanding ionic conductivities in a wide temperature range, superior polarization behavior, remarkable reversibility and more strikingly, excellent compatibility with different sulfur containing and intercalation cathodes: S_8@activated carbon cloth (ACC/S), sulfur poly(acrylonitrile) (SPAN) composite, titanium disulfide, Chevrel phase Mo_6S_8 and lithium titanate. The effective suppression of the 'polysulfide shuttle' by the GPE allows for a stable cycling of Mg||SPAN and Mg||ACC/S cells at room temperature with high discharge capacities (600 and 420 mAh•g_S^{-1} after 140 and 50 cycles, respectively). Remarkably, the Mg||GPE||SPAN system features low self-discharge, excellent flexibility and safety characteristics, which significantly improve the possibility for practical applications.

1. Introduction

Current electric energy storage technology in electric vehicles is mostly based on lithium-ion batteries. However, considering both safety issues and the limited resources of raw materials for lithium batteries, rechargeable magnesium batteries have received considerable attention as a viable alternative by virtue of their improved safety and high earth-abundancy of the electrode material [1]. Growing attention has recently been devoted to Mg-S batteries owing to the low toxicity and the high theoretical volumetric energy density (3200 Wh•L^{-1}) [2–4]. Several prototypes of Mg-S cells have been developed to prove the concept; however, they are still suffering from some critical issues.

In the reported prototypes, sulfur is generally directly adopted by either physical adsorption (*e.g.* sulfur@microporous carbon [5], sulfur@activated carbon cloth (ACC/S) [6]) or covalently bound to the carbon backbone (*e.g.* sulfur@poly(acrylonitrile) (SPAN) [7–9]). Using bulk sulfur-based cathodes generally results in the loss of active materials, self-discharge and severe polysulfide shuttle [8, 10]. Complementary, several groups reported on the use of SPAN-based cathodes in Mg batteries. Similar to lithium-sulfur batteries, the different sulfur species occurring can be better controlled due to the covalently bound sulfur in the carbon matrix [7-9, 11]. The development of electrolytes so far still focused on liquid systems, such as the halogen-containing magnesium aluminum chloride complex (MACC) or magnesium tetrakis(hexafluoroisopropyloxy) ($Mg[B(hfip)_4]_2$) electrolytes [6, 12, 13]. Here, for the first time, the polysulfide shuttle as well as cell leakage and safety problems can be greatly reduced by the combination of SPAN with a halogen-free quasi-solid-state Mg^{2+}/Li^{+} dual salt electrolyte system.

* Corresponding author.
E-mail address: michael.buchmeiser@ipoc.uni-stuttgart.de (M.R. Buchmeiser).

https://doi.org/10.1016/j.ensm.2022.04.034
Received 9 February 2022; Received in revised form 12 April 2022; Accepted 20 April 2022
Available online 22 April 2022

Mg-S cells are in general suffering from the polysulfide shuttle, and poor safety, especially in the combination with conventional bulk sulfur-based cathodes. One attractive way to reduce the polysulfide shuttle that has already been employed in Li-S batteries entails the use of gel polymer electrolytes (GPEs), by which the diffusion of the polysulfides is hindered and the anode is consequently protected [14]. Apart from polysulfide suppression, GPE also reduces the risk of internal short circuits and electrolyte leakage, which greatly improve the safety of this type of cells [15]. Furthermore, GPEs exhibit a high ion conductivity, especially compared to all-solid state electrolytes [3]. Nonetheless, the application of the concept of GPEs in Mg-S batteries is highly recommended, but rarely investigated so far.

Herein, we present a halogen-free Mg^{2+}/Li^{+} dual-salt borate-based gel polymer electrolyte for Mg batteries, showing high ionic conductivities for a wide operating temperature range and superior electrochemical performance. Most important, the developed electrolyte is compatible with not only different intercalation cathodes, but also various types of sulfur-based cathodes. The electrolyte is prepared *via* a straightforward *in-situ* crosslinking reaction between lithium and magnesium borohydrides and poly(tetrahydrofuran) (PTHF) with TiO_2 nanoparticles as additive, using a glass fiber separator as mechanically stable support (magnesium/lithium/TiO_2 GPE, *referred to MLT-GPE*). This electrolyte exhibits superior compatibility with Mg anodes and shows negligible overpotential (<0.06 V) over more than 1100 cycles. The successful suppression of the polysulfide shuttle by the MLT-GPE allows for a stable room/low temperature cycling of Mg||MLT-GPE||SPAN and Mg||MLT-GPE||ACC/S cells with approx. 600 $mAh \bullet g_s^{-1}$ and 420 $mAh \bullet g_s^{-1}$, respectively. More important, the Mg||MLT-GPE||SPAN system shows low self-discharge, excellent flexibility and greatly improved safety issues. Additionally, the MLT-GPE is also well compatible with various intercalation cathodes at ambient temperature, like Mg||MLT-GPE||Mo_6S_8, Mg||MLT-GPE||TiS_2 and Mg||MLT-GPE||LTO ($Li_4Ti_5O_{12}$) cells, which all show excellent cycle stability and high discharge capacities.

2. Results and discussion

2.1. Characterization of the MLT-GPE

For the successful realization of the halogen-free GPE, we took advantage of the high basicity of borohydrides, which allows for a crosslinking reaction with the hydroxyl group in poly(tetrahydrofuran) (PTHF) [15]. More important, the utilization of a Mg^{2+}/Li^{+} dual salt electrolyte in a Mg battery has not only been shown to greatly improve the kinetics of the bivalent Mg^{2+} ions, but also to reduce the passivation of the Mg anode from the sulfur species in a sulfur battery, especially short-chain polysulfides, which have been studied in detail previously [8, 9, 16]. Furthermore, it has been reported that the addition of nano-sized TiO_2 particles can significantly improve the ionic conductivity and mechanical properties of the Mg solid-state electrolyte [17, 18]. Moreover, the formed polysulfide species in sulfur batteries are reported to be successfully trapped by nano-sized TiO_2. Consequently, a better capacity retention and a protected anode can be achieved [17, 18]. We therefore designed a reaction system based on $Mg[BH_4]_2$, Li$[BH_4]$, TiO_2 and PTHF, which reacts *in-situ* in a glass fiber separator, resulting in a gel-like electrolyte (Figure 1a). Also, due to the evolution of hydrogen, a porous structure forms (Fig. 1b), which possesses a different morphology than the pristine glass fiber separator (Fig. S1a).

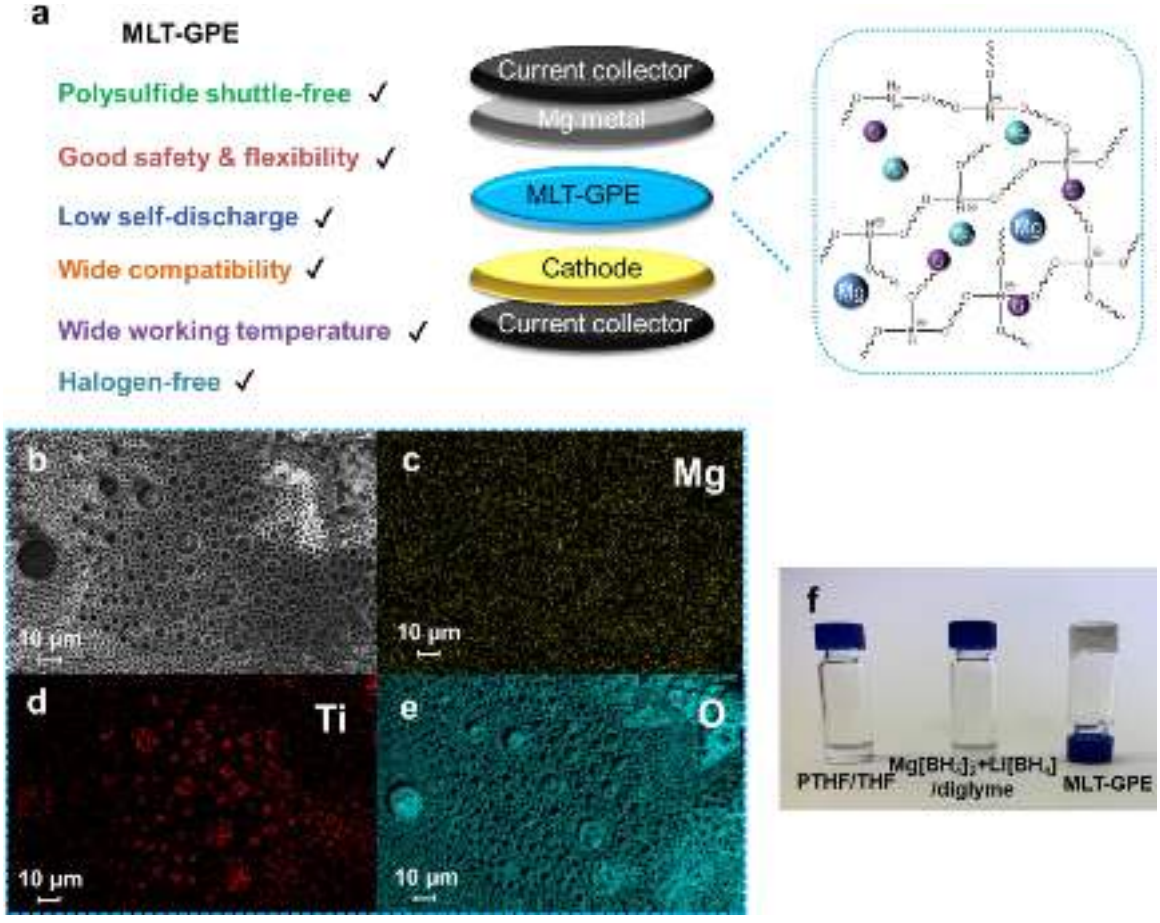

Fig. 1. a) Drawing of a magnesium cell with the crosslinked MLT-GPE; **b-e)** SEM image and elemental mappings of the MLT-GPE**; f)** photographs of the PTHF/THF solution (left), $Mg[BH_4]_2$-Li$[BH_4]$/diglyme solution (middle) and MLT-GPE (right).

The bubbles inside the GPE are a result of the evolution of hydrogen and might have an influence on the properties of the MLT-GPE; hence control over the amount and distribution of the bubbles is important. Indeed, the bubbles might be removed by the application of low vacuum during synthesis. In addition, elemental mapping of the MLT-GPE (Fig. 1c-1e) confirms that all the elements are homogeneously distributed. For clarity, the components of the pristine glass fiber separator (Na, Si) have been neglected. Fig. 1f clearly demonstrates that the liquid hybrid borohydride electrolyte (middle) reacts with the liquid PTHF/THF solution (left), resulting in the immobilized GPE (right). This was additionally confirmed by the cross-section scanning electron microscopy (SEM) images of the MLT-GPE (Fig. S1b, S.I.), where the glass fiber skeletons are thoroughly infiltrated by the cross-linked GPE and become almost invisible. Further on, thermal stability analysis (Fig. S2, S.I.) indicates good thermal stability of the MLT-GPE, which could be attributed to the crosslinked polymer network [15].

Ionic conductivity is an important parameter to evaluate the feasibility and efficiency of a solid-state electrolyte, since it can quantify the ion mobility inside the electrolyte. The ionic conductivities of the MLT-GPE were measured in a temperature range of 0°C to 40°C using electrochemical impedance spectroscopy (EIS) employing an MLT-GPE sandwiched between two stainless steel (SS) plates. The Nyquist plot (Fig. 2a) shows straight lines without semi-circles in the high frequency range. This indicates that only ions are the current carrier and the obtained conductivity is based solely on ion conductivity, which has also been observed in other solid-state batteries [19–21]. This could be

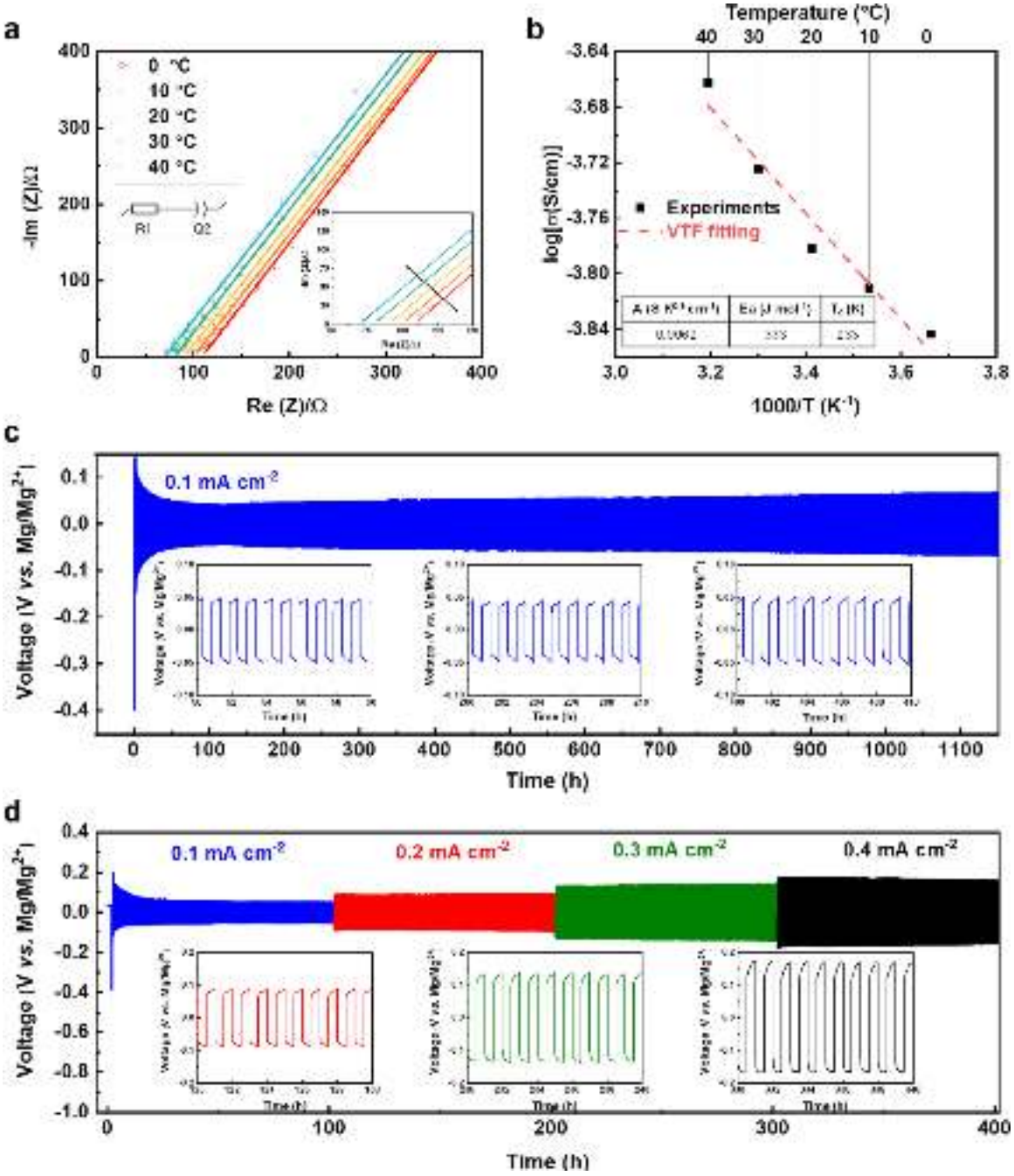

Fig. 2. **a)** Nyquist plots of SS||MLT-GPE||SS at various temperatures; dots: measured values; lines: fitted values (by the inset model); **b)** temperature-dependent ionic conductivity for MLT-GPE; **c)** long-term galvanostatic cycling of a Mg||MLT-GPE||Mg symmetric cell at a current density of 0.1 mA•cm^{-2}; **d)** galvanostatic cycling test of a Mg||MLT-GPE||Mg symmetric cell at various current densities.

attributed to the low glass transition temperature (T_g) of the MLT-GPE (9°C), which ensures a high mobility of the polymer segments and fast relaxation at the high frequency region [20]. The Nyquist plots were fitted using the equivalent circuit model shown in the inset of Fig. 2a; the corresponding fitted values are listed in Table S1. The ionic conductivity increased from 0.15 mS•cm^{-1} to 0.22 mS•cm^{-1} when the temperature was increased from 0°C to 40°C. In addition, the temperature-dependent ionic conductivity follows the Vogel-Tammann-Fulcher (VTF) empirical equation (Eq. (1)) [22]:

$$\sigma = AT^{-0.5} exp\left[\frac{-E_a}{R(T-T_0)}\right] \quad (1)$$

where A is the pre-factor of the ionic conductivity; E_a is the activation energy which is related to the mobility of the polymer chains; T_0 is the temperature which is normally 10 K to 50 K below T_g of the polymer; R is the ideal gas constant [15]. The parameters according to the VTF fitting are listed in the inset of Fig. 2b. The super-low activation energy (0.333 kJ•mol^{-1}) indicates a low energy barrier for the movements of the cations. The calculated T_0 is 233 K, which is 49 K below the T_g (282 K).

In addition, symmetric Mg||Mg cells with MLT-GPE were fabricated to investigate the polarization behavior (Fig. 2c and 2d). Fig. 2c shows that the MLT-GPE exhibits an extremely low overpotential (< 0.06 V) and very good long-term cycling durability (> 1100 cycles) at room temperature. The polarization behavior of the MLT-GPE at higher/different current densities was also evaluated (Fig. 2d) by a Mg||Mg cell. When the current density was successively increased from 0.1 mA•cm^{-2} to 0.4 mA•cm^{-2}, the overpotential of the MLT-GPE did not exceed 0.2 V, confirming the excellent polarization behavior of the MLT-GPE. Additionally, the enlarged potential curves shown in the insets of Fig. 2c, 2d generally show flat features, indicating a smooth Mg plating and stripping. Noticeably, a high overpotential of ca. -0.4 V can be observed in the initial few cycles, followed by a substantial decrease over cycling, which has also been observed in the cases of many liquid magnesium electrolytes [6–8]. To understand this phenomenon, EIS analysis was applied for the Mg||MLT-GPE||Mg symmetric cell before and after cycling (Fig. S3, S.I.). A well-defined semi-circle was observed in the high frequency region after cycling, indicating that an equilibrium state and a perfect contact between the MLT-GPE and the Mg metal have been reached [21]. More important, a sharp decrease of the interfacial resistance after cycling was recorded. Obviously, the adsorption layer and the intrinsic oxide layer on the Mg surface that cause the initial high overpotential, were reduced through the Mg plating and stripping.

Next, the influence of TiO_2 nanoparticles on the electrochemical performance was examined. At first, the ionic conductivity of the GPE without TiO_2 was determined using the same method as for the MLT-GPE (Fig. S4 and Table S2, S.I.). Upon the addition of 10 wt% of TiO_2 nanoparticles, the ionic conductivity increased by one order of magnitude at all temperatures, which is in line with previous studies [17, 18]. Additionally, the magnesium plating/stripping behavior of the GPE with and without TiO_2 nanoparticles was compared using symmetric Mg||Mg and Mg||stainless steel (SS) cells, respectively (Figure S5, Figure S6, S.I.). Addition of the TiO_2 nanoparticles substantially decreased the overpotential from 0.15 V to 0.05 V and increased the oxidative peak current. In view of the positive influence of TiO_2 nanoparticles on electrochemical performance, the following studies focused on GPEs containing 10 wt.% TiO_2.

The oxidative stability of the MLT-GPE was tested with different current collectors by linear sweep voltammetry (LSV, Fig. S7a, S.I.). The MLT-GPE was stable up to 3.5 V on the standard SS current collector, which was further applied as the current collector for the cathode materials. In addition, the reversibility of the MLT-GPE was examined by plating/stripping of Mg on the SS substrate. Fig. S7b (S.I.) displays the cyclic voltammetry (CV) curves between -1 V to 2 V, showing almost overlapping curves from the initial cycle. Furthermore, the Coulombic efficiency of the MLT-GPE was determined (Fig. S7c, S.I.) and turned out to be stable at ~99.8%. Also, the transference number of Mg^{2+} in a pure magnesium electrolyte was measured by EIS (Fig. S8 and Table S3, S.I.), revealing a good transference number of 0.5 [23].

2.2. Mg-SPAN battery performance with the MLT-GPE

To examine the electrochemical performance of the Mg-S batteries, SPAN was first selected as cathode material to test its compatibility with the MLT-GPE, because SPAN (see Fig. 3b inset) has been reported to show good capacity retention in magnesium batteries due to its covalently bound sulfur, which in turn can be well immobilized in the cathode [8, 11]. The SPAN cathodes, comprising SPAN active material, a conventional binder PVDF and conductive carbon black, were analyzed by SEM and elemental mapping (Fig. S9, S.I.), showing good homogeneity. The SPAN cathode was then applied in a Swagelok-type cell together with a polished Mg foil and the MLT-GPE. The Mg||MLT-GPE||SPAN cell was charged and discharged at 0.2 C at 22°C for long-term cycling testing (1 C = 1672 mA•g_s^{-1}, Fig. 3a, voltage curves in Fig. S10, S.I.). The cell delivered an initial discharge capacity of 908 mAh•g_s^{-1} and showed a slight capacity decay within the initial 10 cycles (*ca.* 750 mAh•g_s^{-1} at the 10th cycle). After that, the cell cycled stable for another 130 cycles, with only 0.1% capacity decay per cycle, indicating superior capacity retention (*ca.* 580 mAh•g_s^{-1} at 140th cycle). These values are so far unprecedented in a quasi-solid-state Mg-S battery, even compared to current state of the art Mg batteries based on liquid electrolytes (Table S4, S.I.) [2, 24]. Generally, the capacity contribution from the MLT-GPE is believed to be negligible. In order to verify this, a cell with a Mg anode, an SS current collector as cathode and MLT-GPE as the electrolyte was cycled using the same electrochemical conditions as the previous Mg||SPAN cells (Fig. S7d, S.I.), showing indeed negligible discharge/charge capacities (<1 mAh•g^{-1}). Also, CV curves of the Mg||MLT-GPE||SS cell in Fig. S7d (S.I.) inset do not show any redox peaks in the applied voltage window. Based on these investigations, one can conclude that the capacities from the Mg||MLT-GPE||SPAN cells solely stem from SPAN, but not from the electrolyte.

The cell resistance of the Mg||MLT-GPE||SPAN cell after each cycle at the charged state was also recorded *in-situ*. The corresponding Nyquist plot and the fitted values are shown in Fig. S11 and Table S5, S.I., respectively. The bulk resistance (R_1) in the high frequency region increased slightly, which can be attributed to the formation and dissolution/accumulation of magnesium polysulfides on the MLT-GPE. However, the resistance of the solid electrolyte interphase (SEI) layer (R_2) at the middle frequency range stayed almost constant and low during cycling, indicating the formation of a stable SEI layer on the Mg surface. This implies that the formed sulfide species do not passivate or interact with the Mg metal anode but are instead blocked by the MLT-GPE, leading to a 'polysulfide shuttle-free' system. A comparison of the cycling performance of Mg||SPAN cells using the MLT-GPE and the liquid electrolyte, respectively (Fig. S12, S.I.), revealed that with the liquid electrolyte (0.1 M $Mg[BH_4]_2$, 1.5 M $Li[BH_4]$, 10 wt% TiO_2 in diglyme), the cell showed high discharge capacities (~1150 mAh•g_s^{-1}) in the initial three cycles, implying better sulfur utilization due to the liquid electrolyte. However, the discharge capacity sharply decreased to only ~450 mAh•g_s^{-1} in the 50th cycle, indicating poorer sulfur addressability and capacity retention compared to cells based on the MLT-GPE. These findings again confirm the successful suppression of the polysulfide shuttle by the MLT-GPE.

In addition, the aged Mg anode removed from the MLT-GPE electrolyte after 10 cycles was investigated by *ex-situ* X-ray photoelectron spectroscopy (XPS, Fig. 3e and f). On the aged Mg anode, a thin layer consisting of several sulfur species was identified in the S 2p spectra. Apart from a sulfone species (~169 eV), only magnesium polysulfides (MgS_x) (~163.6 eV) were detected. These magnesium polysulfides originate most likely from the residual GPE, which is hard to remove due to its gel-like structure. Notably, no MgS, which is the major harmful species leading to the shuttle effect since it is hard to be re-oxidized

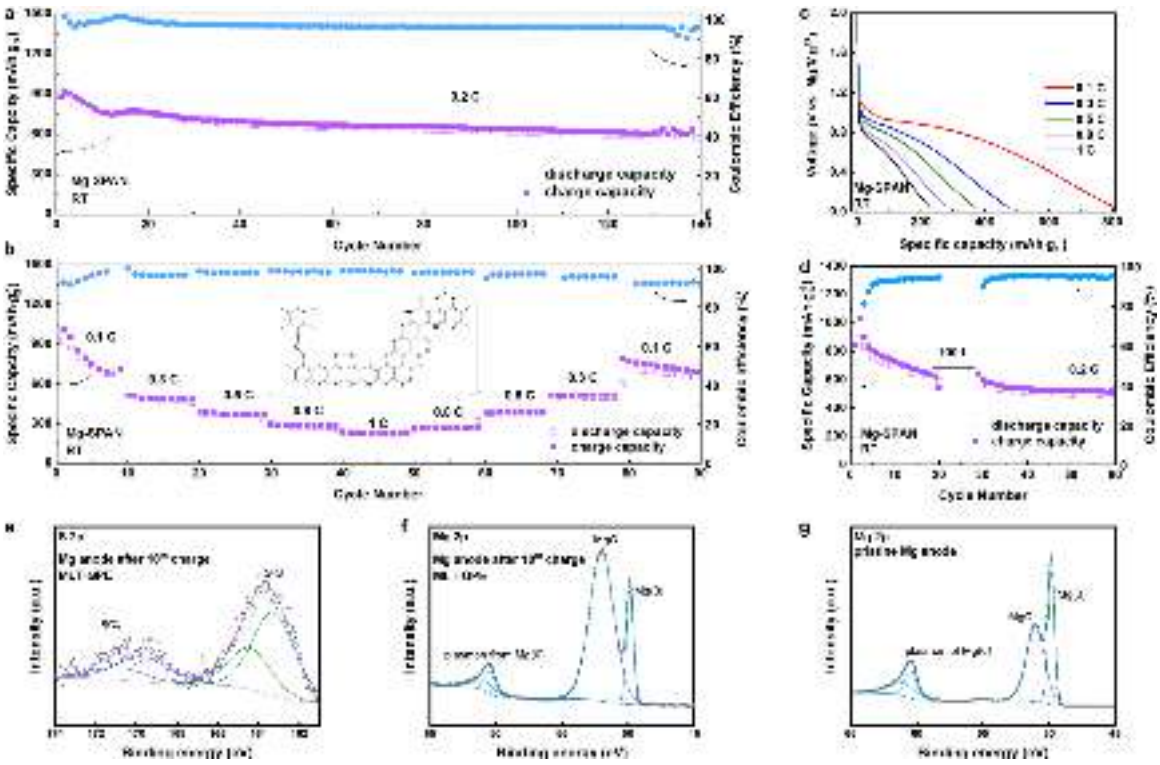

Fig. 3. a-d) Electrochemical characterization of a Mg||MLT-GPE||SPAN cell at room temperature (RT, 22°C); **a)** long-term galvanostatic cycling (charging/discharging at 0.2 C); **b)** rate capability test from 0.1 C to 1 C; inset: chemical structure of SPAN; **c)** corresponding potential curves at different current densities; **d)** self-discharge analysis of the Mg||MLT-GPE||SPAN cell; **(e)** S 2p XPS spectra of a cycled Mg anode; **(f)** Mg 2p XPS spectra of an aged Mg anode after 10 cycles in the charged state using an MLT-GPE electrolyte; **g)** Mg 2p XPS spectra of a pristine Mg anode.

during charging [16, 25], was found on the aged Mg anode at ~160 eV [9]. The absence of MgS on the aged Mg anode strongly suggests that the Mg anode is well protected, which helps in the successful suppression of the shuttle effect by the MLT-GPE [9].

According to our previous study, the addition of a lithium salt to a magnesium electrolyte can significantly improve the redox kinetics, increase the solubility of the magnesium (poly)sulfides by lithiation and reduce the passivation of the Mg anode [9]. At the same time, it is important to know whether lithium species join the redox reaction. To obtain more direct chemical proof of the redox chemistry, *ex-situ* XPS was applied to both, pristine and aged Mg anodes. Fig. 3f and g shows the XPS spectra of an aged Mg anode cycled in the MLT-GPE electrolyte in the charged state and of a pristine Mg anode. Both spectra show similar features; Mg(0) and MgO species can be detected at approx. 49.8 eV and 51 eV, respectively. Importantly, no peaks were found at about 55.3 eV, where the Li 1s signal would be expected [9]. This indicates that no lithium species, especially lithium metal, are formed during cycling. Consequently, the entire redox process is solely governed by the Mg chemistry, which is in line with results reported for Mg batteries using Li-containing liquid electrolytes [8, 9, 16, 26]. Due to the strong physical interaction between the MLT-GPE and the SPAN cathode coating, *post-mortem* analysis of the SPAN cathode could not be conducted.

Next, the rate capability of the Mg||MLT-GPE||SPAN cell was also evaluated by charging and discharging the cell at different current rates at room temperature. As depicted in Fig. 3b, the battery delivered a capacity of ca. 800, 480, 380, 290 and 230 mAh•g_s^{-1} at current rates of 0.1, 0.3, 0.5, 0.8 and 1 C, respectively. The capacity successfully reversed back when the current rate decreased, demonstrating the superior rate capability of the Mg||MLT-GPE||SPAN system. Fig. 3c shows the discharge profile of a Mg||MLT-GPE||SPAN cell at various current rates. Only one smoothly sloped profile around 1 V instead of several plateaus in conventional bulk sulfur cells can be observed. This sloped voltage profile is characteristic for SPAN cathodes and is in good agreement with the voltage profiles observed in solid-state Li-SPAN cells and liquid-state Mg-SPAN cells [7, 9, 27, 28].

Low temperature durability is another important factor for any practical use of a battery system. Thanks to the relatively high ionic conductivity of the MLT-GPE at low temperatures, the performance of the Mg||MLT-GPE||SPAN cell was also examined at 0°C. The cells stably delivered a considerably high discharge capacity of approx. 300 mAh•g_s^{-1} (Fig. S13a, S.I.). The rate capability of the Mg||MLT-GPE||SPAN cell was also investigated at 0°C, cycling between 0.1 C and 1 C (Fig. S13b, S.I.). Although the cell delivered lower discharge capacity at a higher current rate, which might be due to the lower diffusivity, the capacity was still able to return back when the current rate decreased, showing relatively good rate capability. These data illustrates the wide application temperatures of the Mg||MLT-GPE||SPAN cell.

Furthermore, CV measurements of the Mg||MLT-GPE||SPAN cell at different scan rates (Fig. S14a, S.I.) revealed one distinct oxidation peak starting from 1.4 V and one reduction peak starting from 1.1 V. The redox peak positions are in good agreement with the voltage plateaus in Fig. 3c, indicating the redox reactions between SPAN and lower-order poly(sulfides). Also, the current densities of the redox peaks increase linearly with an increasing scan rate in a double logarithmic diagram (Fig. S14b, S.I.), indicating that both redox reactions are diffusion-controlled and not surface-limited adsorption processes [29].

The extent of self-discharging is another crucial feature in the evaluation of energy-storage devices, especially with sulfur batteries using ether-based electrolytes, such as DME or diglyme [30]. The extent of self-discharge of the Mg||MLT-GPE||SPAN cell was investigated by resting the cell in the fully charged state after 20 cycles for 100 hours (Fig. 3d). After 100 hour resting time, the cell still stably delivered ca. 580 mAh•g_s^{-1}, showing negligible capacity decay, indicating the absence of any self-discharge.

Besides its electrochemical performance, safety is one of the most

important aspects of a battery system. In order to further examine the safety properties of the Mg||MLT-GPE||SPAN system, soft package Mg||MLT-GPE||SPAN (Pouch) cells were assembled and tested. In Fig. 4a, using two Mg||MLT-GPE||SPAN cells connected in series, a red light emitting diode (LED) light can be successfully lightened up. Moreover, the situation when the cells are under external mechanical force was examined by bending one or even both of the Pouch cell(s). As shown in Fig. 4b and in the video (Supporting Information), the LED is still successfully lightened with the same brightness, indicating the excellent flexibility of the Mg||MLT-GPE||SPAN pouch cells.

Further on, the soft-package cell was half-cut, as shown in Fig. 4c. The cell was still capable of powering the LED light, illustrating that cutting does not lead to an internal-short circuit. Fig. 4d shows the cross-section of the cut Mg||MLT-GPE||SPAN cell, where a gel-like structure instead of liquid leakage can be observed. All of these experiments show that the Mg||MLT-GPE||SPAN batteries possess excellent safety characteristics.

2.3. Performance of Mg-sulfur/ion batteries with an MLT-GPE

The outstanding electrochemical performance of the Mg||MLT-GPE||SPAN cell encouraged us to further examine the polysulfide suppression effect of the MLT-GPE with a conventional elemental sulfur system. A binder-free cathode, i.e. sulfur@activated carbon cloth (ACC/S), which has already been applied in several metal-sulfur systems, was employed in a magnesium battery together with the MLT-GPE. The Mg||MLT-GPE||ACC/S cell was also cycled at 0.2 C at room temperature. As shown in Fig. 5a and Fig. S15a (S.I.), the cell delivered an initial discharge capacity of around 600 mAh•g_s^{-1} at 0.2 C. Strikingly, the cell then delivered an almost constant capacity of 420 mAh•g_s^{-1} for more than 50 cycles with >99% Coulombic efficiency. In sharp contrast, the Mg||ACC/S cell with the liquid electrolyte (0.1 M $Mg[BH_4]_2$, 1.5 M Li$[BH_4]$, 10 wt% TiO_2 in diglyme) delivered a higher initial discharge capacity (~800 mAh•g_s^{-1}) due to a better sulfur utilization (Fig. 5b). However, from the third cycle on, the cell showed very poor Coulombic efficiency (<60%), caused by a severe polysulfide shuttling compared to the Mg||liquid electrolyte||SPAN system. Clearly, the SPAN structure retains sulfur much better than the free elemental sulfur system in a liquid electrolyte. Nonetheless, the MLT-GPE was capable of suppressing the polysulfide shuttle in a sulfur cell, resulting in a stable system with good capacity retention.

Intercalation cathode materials are also good candidates for rechargeable magnesium batteries beyond sulfur cathodes [31–33]. A feasible and practical electrolyte should show good electrochemical performance and also good compatibility with these electrodes. To verify the compatibility of the MLT-GPE with intercalation cathode materials, the MLT-GPE was also utilized in several types of intercalation cathodes, namely Chevrel phase Mo_6S_8 (Fig. S16, S.I.), TiS_2 and spinel $Li_4Ti_5O_{12}$ (LTO) cathodes. As shown in Fig. 5c and Fig. S17a (S.I.), the Mg||MLT-GPE||TiS_2 cell stably delivered 235 mAh•g^{-1} with approximately 98% Coulombic efficiency at 0.5 C at room temperature. (1 C = 239 mA•g^{-1}) for 70 cycles, representing outstanding specific capacities and cycle stability. In the rate capability test, the cell delivered discharge capacities of 235, 205, 190, 180 mAh•g^{-1} at 0.5 C, 1 C, 2 C and 3 C, respectively (Fig. 5d and Fig. S17b, S.I.). The capacity fully recovered when the current rate decreased, demonstrating the good rate capability of the system. The corresponding voltage profiles and the CV curves (Fig. S17c, S.I.) show two distinct plateaus at 1.4 V and 0.9 V during discharge, indicating the stepwise intercalation of Mg into the TiS_2 lattice. The observed plateaus are in line with the reported Mg-TiS_2 cells with the liquid all phenyl complex (APC) electrolyte characterized *via in-situ* methods [31]. Overall, excellent compatibility of the MLT-GPE with the insertion cathodes was observed.

As a step further, spinel $Li_4Ti_5O_{12}$ (LTO), which is known as a "zero-strain" ion insertion-type anode material for the full cell applications, was utilized as electrode material together with Mg metal and the MLT-GPE to examine its possible application for Mg full cells [34, 35]. Fig. 5e displays the Mg||MLT-GPE||LTO cell cycled at 0.2 C (1 C = 175 mAh•g_{LTO}^{-1}) at room temperature. The discharge capacity increased from 80 to 120 mAh•g_{LTO}^{-1} over the initial 10 cycles and stayed almost constant during the following 60 cycles with 99.5% Coulombic efficiency, resulting in ca. 100 mAh•g_{LTO}^{-1} at the 70th cycle. The increase in capacity during the initial cycles is attributed to the decrease of polarization over cycling, as can be deduced from the corresponding voltage profiles (Fig. S18a, S.I.) and the CV curves (Fig. S18c, S.I.). Additionally, the Mg||MLT-GPE||LTO cell delivered 110, 105, 85, 70 mAh•g_{LTO}^{-1} at 0.2, 0.5, 1 and 2 C, respectively (Fig. 5f). The capacity also fully recovered with a decreasing current rate, indicating outstanding rate capability of the system. The potential curves of the cell (Fig. S18a,b, S.I.) display distinct plateaus at 0.8 V and 0.9 V during discharge and charge, respectively, which show very similar characteristic with the Mg||LTO system based on a lithium-containing liquid electrolyte [34]. The role of the lithium salt in a magnesium electrolyte for the applications of magnesium ion batteries was discussed already in several publications [26, 33, 34]. To date it is assumed that reversible magnesium plating/stripping takes only place at the anode side due to the thermodynamic redox potential difference between Mg^{2+}/Mg and Li^+/Li in a Mg^{2+}/Li^+ hybrid electrolyte [33, 34].

3. Experimental Section

3.1. Chemicals

All samples were handled inside an Ar-filled glovebox with H_2O and O_2 levels ≤ 0.1 ppm. All cells were fabricated in the same glovebox. Glassware was dried in an oven at 120°C. Magnesium borohydride (Mg$[BH_4]_2$, 95%), lithium borohydride (Li$[BH_4]$, >95%), anhydrous diethyleneglycol dimethyl ether (diglyme, 99.5%), poly(tetrahydrofuran)

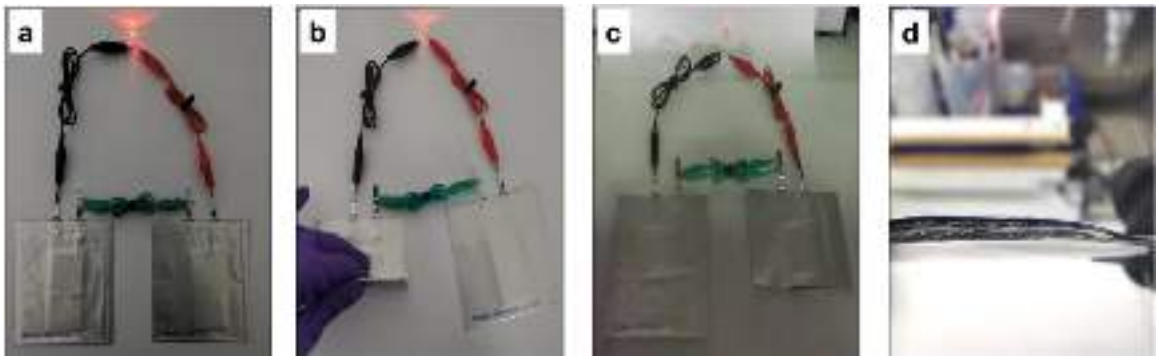

Fig. 4. a-d) Illustrations of two soft-package Mg||MLT-GPE||SPAN cells connected in series at room temperature **a)** at normal conditions; **b)** under bending conditions; **c)** after cutting one cell; **d)** cross-section of the cut soft package cell.

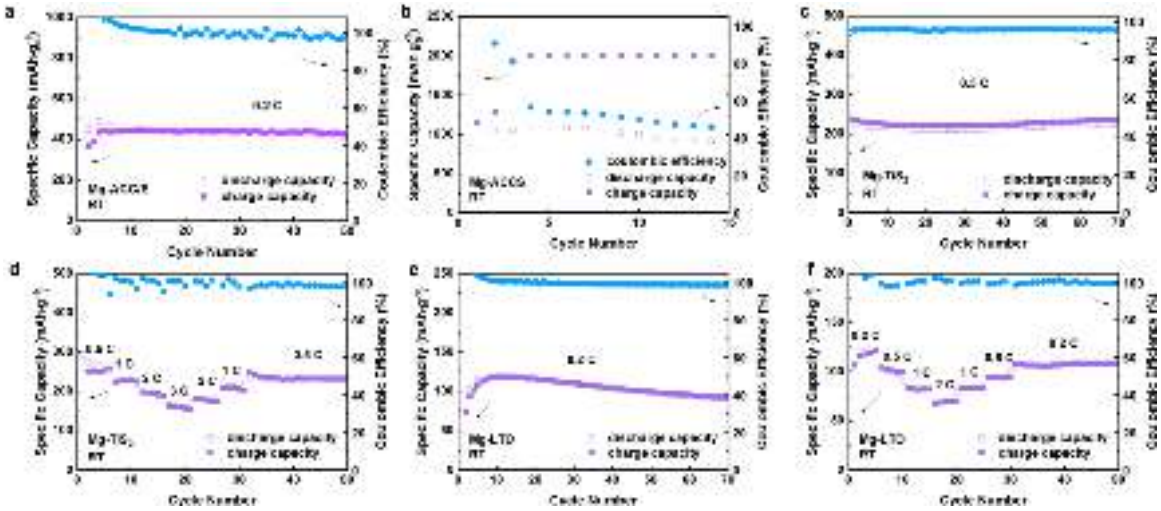

Fig. 5. Compatibility of the MLT-GPE with bulk sulfur-based and intercalation cathodes: **a)** long-term cycling stability test of Mg||MLT-GPE||ACC/S cell at room temperature, charging/discharging at 0.2 C; **b)** long-term cycling stability test of Mg||liquid electrolyte||ACC/S cell at room temperature, charging/discharging at 0.2 C; **c)** cycle stability test of Mg||MLT-GPE||TiS_2 cells, charge/discharge at 0.5 C (1 C = 239 mA•g^{-1}); **d)** rate capability test Mg||MLT-GPE||TiS_2 cells from 0.5 C to 3 C; **e)** cycle stability test of Mg||MLT-GPE||LTO cells, charge/discharge at 0.2 C (1 C = 175 mA•g^{-1}); **f)** rate capability test of Mg||MLT-GPE||LTO cells from 0.5 C to 3 C. All the cells were characterized at room temperature (22°C).

(PTHF, *M*n~2900 g/mol), titanium dioxide nanopowder (21 nm, ≥99.5% trace metals basis), titanium disulfide (TiS_2), lithium titanate (LTO) and poly(acrylonitrile) (PAN, *M*n=36,500 g/mol, Đ=3.6) were purchased from Merck and used as received. Chevrel phase Mo_6S_8 was purchased from NEI Corporation and used as received. Anhydrous tetrahydrofuran (THF) was obtained from Solvent Purification System. Magnesium foils (0.25 mm, 99.9%, Advent Research Materials) were punched into chips 12 mm in diameter and thoroughly scratched with a ceramic knife before use. Glass fiber separators (Whatman, GF/C) were punched into chips 13 mm in diameter and dried at 120°C under vacuum for 40 h.

3.2. Preparation of electrolytes

0.1 M $Mg[BH_4]_2$ and 1.5 M $Li[BH_4]$ solutions in diglyme were prepared inside an Ar-filled glovebox. The preparation method follows our previous reports [8], where the use of this specific salt ratio showed the best electrochemical performance. After one day of stirring, 10 wt% of TiO_2 was added; the mixture is referred to as *MLT/diglyme*.1 g PTHF was then dissolved in 5 mL THF, the solution is referred to as *PTHF/THF*. The gel polymer electrolyte, referred to as MLT-GPE, was synthesized by the *in-situ* crosslinking reaction between MLT/diglyme and PTHF/THF inside the glass fiber separator. The glass fiber separator was used as mechanical reinforcement. In detail, 45 μL MLT/diglyme and 45 μL PTHF/THF were pipetted to one piece of glass fiber separator. Based on the components in the above synthesis, the molar quantities of Mg $[BH_4]_2$, $Li[BH_4]$, and the -CH_2-CH_2-CH_2-CH_2-O- unit from PTHF were 0.0045 mmol, 0.0675 mmol and 0.625 mmol, respectively.

3.3. Preparation of various cathodes

Sulfurized poly(acrylonitrile) composite (SPAN) was synthesized according to the literature [7, 8]. SPAN cathodes were prepared by mixing 70 wt% SPAN powders, 15 wt% super C65 carbon black and 15 wt% poly(vinylidene fluoride) (PVDF) in 1-methyl-2-pyrrolidinone at 2, 000 rpm for 6 minutes with a mixer (Thinky). The obtained slurry was then casted onto a stainless-steel foil with a wet thickness of 300 μm. The coating was dried in an oven at 60°C for 24 h. Cathodes were punched into chips 12 mm in diameter. The average sulfur content was around 0.7~1 mg/cm^2.

For the ACC/S cathode preparation, activated carbon cloth (ACC 507-20, Kynol) was cut in electrodes with 12 mm diameter and dried at 120°C in vacuum for 12 h. In an argon-filled glovebox (O_2 < 1 ppm, H_2O < 1 ppm), sulfur powder (99.5 %, Alfa Aesar) was distributed on the ACC surface (approx. 1.6 mg/cm^2) and melt infiltrated into the microporous carbon at 155°C for 24 h applying an autoclave vessel. Subsequently, the infiltrated ACC/S cathodes were placed in a glass tube under argon atmosphere and transferred to a tubular furnace to evaporate residual sulfur from the carbon surface at 330°C for 3 h (5 K/min heating rate). Thus, ACC/S cathodes with a sulfur loading of approx. 0.6 mg/cm^2 result.

TiS_2 insertion cathodes, LTO cathodes and Chevrel phase Mo_6S_8 cathodes were prepared by mixing the active material, super C65 carbon black and poly(vinylidene fluoride) (PVDF) in 1-methyl-2-pyrrolidinone in a weight ratio of 70:15:15, 80:10:10 and 70:15:15, respectively. The slurry was mixed at 2,000 rpm for 6 minutes with a mixer (Thinky) and then casted onto a stainless-steel current collector with a wet thickness of 200 μm, 300 μm and 300 μm, respectively. The coating was dried in an oven at 60°C for at least 24 h. Cathodes were punched into chips 12 mm in diameter. The active material per cathode was around 2 mg, 2 mg and 7.4 mg, respectively.

3.4. Electrochemical measurements

The ionic conductivity of the MLT-GPE was measured by electrochemical impedance spectroscopy on a Biologic VMP-3. The MLT-GPE was sandwiched between two stainless steel electrodes in a Swagelok-type cell. The impedance was recorded in a frequency range between 100 kHz and 100 mHz at different temperatures (0°C to 40°C). The ionic conductivity was calculated by the equation 2:

$$\sigma = \frac{l}{SR} \tag{2}$$

where σ is the ionic conductivity (S/cm); l is the thickness of the MLT-GPE; S is the area of the stainless-steel disc; R is the resistance obtained from the impedance measurement.

The stability of the MLT-GPE was determined by Linear Sweep Voltammetry (LSV) using a Biologic VMP-3. A two-electrode cell with stainless steel foil/graphite foil/platinum foil and Mg foil as electrodes and MLT-GPE as electrolyte was employed and swept at 5 mV/s.

Cyclic Voltammetry (CV) was measured on a Biologic VMP-3 using two-electrode or three-electrode cells comprising stainless steel or SPAN

as working electrodes, freshly polished Mg foil as counter and reference electrodes and MLT-GPE as electrolyte. Scan rates between 0.2 mV/s and 0.8 mV/s were applied.

The electrochemical performance of Mg-S batteries and Mg-ion batteries was evaluated by Swagelok-Type cells comprising the respective cathode material, a freshly scratched Mg foil as anode and MLT-GPE as electrolyte. When preparing the cell, 45 μL MLT/diglyme and 45 μL PTHF/THF were consecutively added to the glass fiber disc. All the cells were allowed to rest for at least 3 hours before testing.

The flexibility and safety of the Mg||MLT-GPE||SPAN system were evaluated with the aid of pouch cells. For their assembly, cathodes (31 × 56 mm^2) and anodes (32.5 × 57 mm^2) of the specified size were obtained by die-cutting. Afterwards, Al tabs (AME energy) were connected to the electrode foils by ultrasonic welding. The separator (Whatman GF/C) was cut into pieces with a size of 67 × 37 mm^2. Before introduction into the glovebox, the electrodes and separators were dried in vacuum at 60°C for 20 h and 80°C for 48 h, respectively. The further cell assembly was carried out in an Argon filled glovebox (O_2 < 1 ppm, H_2O < 1ppm). The Mg anode was first thoroughly scratched with a ceramic knife. Afterwards, the separator was placed on the activated side of the anode. Then, 600 mL MLT/diglyme and PTHF/THF were added dropwise onto the separator, respectively. The cathode was then placed on the separator and the cell stack was stabilized with a chemical-resistant adhesive tape. Finally, the stacks were inserted into a pouch bag (7 × 20 cm^2, 184 μm, DNP), which was afterwards sealed under vacuum.

3.5. Materials characterizations

Scanning electron microscopy (SEM) images and energy dispersive X-ray (EDX) spectra were obtained on an Auriga type field emission scanning electron microscope from Zeiss. The samples were stored in Ar-filled glass vials, and measured under air. For *ex-situ* XPS measurements, the cells were disconnected after ten cycles in the charged state. The pristine Mg anode was thoroughly scratched by a ceramic knife inside a glovebox. The Mg anodes were then washed by DME, dried, and fixed on a sample holder under Ar. Due to the stickiness of the MLT-GPE, some residual electrolyte remained on the Mg anode. The samples were transferred under argon to avoid any contamination with air. XPS measurements were performed on a Kratos Axis Ultra system equipped with a monochromic Al K_α source. Spectra were analyzed using the CasaXPS software. The energy separation and peak area of the S $2p_{3/2}$ and S $2p_{1/2}$ were constrained to 1.18 eV and 2:1, respectively [36].

4. Conclusions

In summary, we outlined the effectiveness of a halogen-free Mg^{2+}/Li^+ dual salt-containing GPE in Mg-S and Mg-ion batteries. The novel design concept effectively solves the major issues in metal-sulfur batteries by reducing the shuttle effect and the risks of electrolyte leakage. The novel MLT-GPE with outstanding electrochemical performance has been synthesized *via* an *in-situ* crosslinking reaction between $Li[BH_4]$, $Mg[BH_4]_2$ and the hydroxyl groups of PTHF in a glass fiber membrane with TiO_2 nanoparticles as additive. The MLT-GPE exhibited high ionic conductivities over a wide temperature range, excellent polarization behavior, good reversibility and outstanding compatibility with sulfur and intercalation cathodes. The Mg||MLT-GPE||SPAN cells and the Mg||MLT-GPE||ACC/S cells showed good cycling stability, rate capability and high discharge capacities by suppressing the polysulfide shuttle. Detailed impedance and XPS, measurements have been conducted to verify the concept. Moreover, the Mg||MLT-GPE||SPAN pouch cells show low self-discharge, good flexibility and safety properties, which benefit the practical use of this system. Further on, the Mg||MLT-GPE||Mo_6S_8 cells, Mg||MLT-GPE||TiS_2 cells and Mg||MLT-GPE||LTO cells all showed superior cycle stability and rate capability at room temperature. The MLT-GPE presented here not only narrows the gap between the lab cells and a practical use, but also sets directions for future developments in the area of high-performance room-temperature rechargeable solid-state magnesium batteries.

CRediT authorship contribution statement

Peiwen Wang: Conceptualization, Data curation, Formal analysis, Investigation, Methodology, Writing – original draft, Writing – review & editing. **Janina Trück:** Resources. **Joachim Häcker:** Resources, Writing – review & editing. **Anja Schlosser:** Methodology, Resources, Writing – review & editing. **Kathrin Küster:** Methodology, Writing – review & editing. **Ulrich Starke:** Methodology, Writing – review & editing. **Leonie Reinders:** Methodology, Writing – review & editing. **Michael R. Buchmeiser:** Funding acquisition, Project administration, Supervision, Validation, Writing – review & editing.

Declaration of Competing Interest

The authors declare no competing financial interests or personal relationships that could have appeared to influence the work reported in this paper.

Acknowledgment

We gratefully acknowledge financial support by the German Federal Ministry of Education and Research (project number 03XP0208J) and by the German Federal Ministry of Economic Affairs and Energy (project number 03ETE003E). The authors would also like to thank the Ministry of Science, Research and Arts of the Federal State of Baden-Württemberg for financial support within the InnovationsCampus Mobilität der Zukunft. We also wish to thank Mr. U. Hageroth from the German Institutes of Textile and Fiber Research (DITF), Denkendorf, for SEM/EDX measurements. We also acknowledge Dr. Annika Baumann from EL-Cell GmbH and Mr. Felix Kampmann from Schäffler Technologies AG & Co. KG for the kind material supplement.

Supplementary materials

Supplementary material associated with this article can be found, in the online version, at doi:10.1016/j.ensm.2022.04.034.

References

[1] P. Bonnick, J. Muldoon, Adv. Funct. Mater. 30 (2020), 1910510.
[2] P. Wang, M.R. Buchmeiser, Adv. Funct. Mater. 29 (2019) 1905248–1905275.
[3] P.W. Jaschin, Y. Gao, Y. Li, S.-H. Bo, J. Mater. Chem. A 8 (2020) 2875–2897.
[4] Y. Lu, C. Wang, Q. Liu, X. Li, X. Zhao, Z. Guo, Small Methods 5 (2021), 2001303.
[5] W.Q. Wang, H.C. Yuan, Y. Nuli, J.J. Zhou, J. Yang, J.L. Wang, J. Phys. Chem. C 122 (2018) 26764–26776.
[6] Z. Zhao-Karger, R. Liu, W. Dai, Z. Li, T. Diemant, B.P. Vinayan, C. Bonatto Minella, X. Yu, A. Manthiram, R.J. Behm, M. Ruben, M. Fichtner, ACS Energy Lett 3 (2018) 2005–2013.
[7] P. Wang, J. Kappler, B. Sievert, J. Häcker, K. Küster, U. Starke, F. Ziegler, M. R. Buchmeiser, Electrochim. Acta 361 (2020), 137024.
[8] P. Wang, J. Trück, S. Niesen, J. Kappler, K. Küster, U. Starke, F. Ziegler, A. Hintennach, M.R. Buchmeiser, Batter. Supercaps 3 (2020) 1239–1247.
[9] P. Wang, K. Küster, U. Starke, C. Liang, R. Niewa, M.R. Buchmeiser, J. Power Sources 515 (2021), 230604.
[10] L. Kong, C. Yan, J.-Q. Huang, M.-Q. Zhao, M.-M. Titirici, R. Xiang, Q. Zhang, Energ. Environ. Mater. 1 (2018) 100–112.
[11] S. Zhang, Y. Huang, Y. NuLi, B. Wang, J. Yang, J. Wang, J. Phys. Chem. C 124 (2020) 20712–20721.
[12] J. Luo, S. He, T.L. Liu, ACS Energy Lett 2 (2017) 1197–1202.
[13] Y. Yang, W. Wang, Y. Nuli, J. Yang, J. Wang, ACS Appl. Mater. Interfaces 11 (2019) 9062–9072.
[14] S. Li, W. Zhang, J. Zheng, M. Lv, H. Song, L. Du, Adv. Energy Mater. 11 (2020), 2000779.
[15] A.B. Du, H.R. Zhang, Z.H. Zhang, J.W. Zhao, Z.L. Cui, Y.M. Zhao, S.M. Dong, L. L. Wang, X.H. Zhou, G.L. Cui, Adv. Mater. 31 (2019), 1805930.
[16] T. Gao, M. Noked, A.J. Pearse, E. Gillette, X. Fan, Y. Zhu, C. Luo, L. Suo, M. A. Schroeder, K. Xu, S.B. Lee, G.W. Rubloff, C. Wang, J. Am. Chem. Soc. 137 (2015) 12388–12393.
[17] F. Lee, M.-C. Tsai, M.-H. Lin, Y.L. Ni'mah, S. Hy, C.-Y. Kuo, J.-H. Cheng, J. Rick, W.-N. Su, B.-J. Hwang, J. Mater. Chem. A 5 (2017) 6708–6715.

[18] R. Deivanayagam, M. Cheng, M. Wang, V. Vasudevan, T. Foroozan, N.V. Medhekar, R. Shahbazian-Yassar, ACS Appl. Energy Mater. 2 (2019) 7980–7990.
[19] K. Karuppasamy, P.A. Reddy, G. Srinivas, R. Sharma, A. Tewari, G.H. Kumar, D. Gupta, J. Solid State Electrochem 21 (2016) 1145–1155.
[20] B. Huang, Y. Zhang, M. Que, Y. Xiao, Y. Jiang, K. Yuan, Y. Chen, RSC Adv., 7 (2017) 54391–54398.
[21] G.P. Pandey, R.C. Agrawal, S.A. Hashmi, J. Solid State Electrochem. 15 (2010) 2253–2264.
[22] S. Huang, Z. Cui, L. Qiao, G. Xu, J. Zhang, K. Tang, X. Liu, Q. Wang, X. Zhou, B. Zhang, G. Cui, Electrochim. Acta 299 (2019) 820–827.
[23] Y.G. Cho, C. Hwang, D.S. Cheong, Y.S. Kim, H.K. Song, Adv. Mater. 31 (2019), e1804909.
[24] Z. Ma, D.R. MacFarlane, M. Kar, Batteries & Supercaps 2 (2019) 115–127.
[25] A. Robba, A. Vizintin, J. Bitenc, G. Mali, I. Arčon, M. Kavčič, M. Žitnik, K. Bučar, G. Aquilanti, C. Martineau-Corcos, A. Randon-Vitanova, R. Dominko, Chem. Mater. 29 (2017) 9555–9564.
[26] J. Trück, P. Wang, E. Buch, J. Groos, S. Niesen, M.R. Buchmeiser, J. Electrochem. Soc. 169 (2022), 010505.
[27] S. Zhang, Energy 7 (2014) 4588–4600.
[28] Z. Lin, Z. Liu, W. Fu, N.J. Dudney, C. Liang, Angew. Chem. 125 (2013) 7608–7611.
[29] S. Li, Z. Zeng, J. Yang, Z. Han, W. Hu, L. Wang, J. Ma, B. Shan, J. Xie, ACS Appl. Energy Mater. 2 (2019) 2956–2964.
[30] S. Wei, S. Xu, A. Agrawral, S. Choudhury, Y. Lu, Z. Tu, L. Ma, L.A. Archer, Nat Commun 7 (2016) 11722.
[31] X. Sun, P. Bonnick, L.F. Nazar, ACS Energy Lett 1 (2016) 297–301.
[32] Z.L. Tao, L.N. Xu, X.L. Gou, J. Chen, H.T. Yuan, ChemComm (2004) 2080.
[33] H.D. Yoo, Y. Liang, Y. Li, Y. Yao, ACS Appl. Mater. Interfaces 7 (2015) 7001–7007.
[34] N. Wu, Z.Z. Yang, H.R. Yao, Y.X. Yin, L. Gu, Y.G. Guo, Angew. Chem. Int. Ed. 54 (2015) 5757–5761.
[35] M. Rashad, M. Asif, J. Energy Chem, 56 (2021) 383-390.
[36] J.F. Moulder, W.F. Stickle, P.E. Sobol, K.D. Bomben, Handbook of X-ray Photoelectron Spectroscopy, Physical Electronics Division, Perkin-Elmer Corporation, Minnesota, 1992.